Simulating Complex Satellites and a Space-Based Surveillance Sensor Simulation

Cody R. Singletary and Francis K. Chun
Department of Physics, U.S. Air Force Academy

ABSTRACT

Maintaining space situational awareness requires the ability to track earth-bound satellites in order to know and predict their position, movement, size, and physical features. However, there are many satellites in orbit that are simply too small or too far away to resolve by conventional optical imaging. We can use photometric techniques to gather information about the body in question, but the problem comes in how we interpret the light curve data. Light curves are created by measuring the intensity of reflected sunlight off of the object as it passes overhead. The intensity is dependent on a variety of factors to include the size, shape, orientation, and material composition of the satellite. When we attempt to solve the inverse problem for light curves, we are attempting to extract information about these different factors. Forward modeling of photometric light curves provides a way to generate a large amount of data under controlled conditions for working the inverse problem and is an effective way to test Non-Resolved Space Object Identification (NRSOI) techniques. Currently, there are few implementations of such modeling programs, one of which only allows simple geometric shapes with the option of antennas. We present our modification to that existing code to create complex models plus our new code to calculate shadowing on the complex object. Then we show the results from the new model and a comparison to the original tool. The next generation of space surveillance sensors will be on satellites. Space based sensors avoid many of the problems of ground based sensors, such as, waiting for lighting conditions to match satellite passes and a night sky. These sensors are restricted only by sun exclusion angle and line of sight around the Earth. This allows for more effective techniques and a much longer time on target. We present an addition to the existing code to consider a sensor in orbit. The code is generalized to provide flexibility in testing different orbital parameters and provides pass prediction with predictive forward modeling for any orbit.

1. INTRODUCTION

Space situational awareness is a mission of growing importance for the Air Force and the United States. As more and more countries develop their space capabilities, it will become vital for the U.S. to maintain awareness of all objects orbiting the earth, especially as it pertains to U.S. security and space capability. Being able to track satellites in order to maintain a catalog, will need to evolve into characterizing those satellites. High-resolution imagery of satellites will certainly provide a means of characterization, but as satellites become smaller or as the range to satellites increases, it will become harder and harder to obtain the requisite high-resolution imagery (Fig. 1). Thus other means for characterizing satellites will need to be developed. Research into non-resolvable space object identification techniques is beginning, especially with the adaptation of standard astronomical observational techniques to satellites. Analysis of a satellite's time-varying photometric signature can provide some information on its form, fit, and function.

A satellite's photometric light curve is the intensity of reflected sunlight off of the object as it passes overhead. The intensity is dependent on a variety of factors to include the size, shape, orientation, and material composition of the satellite. When we attempt to invert a satellite's light curve, we are attempting to extract information about these different factors.

Forward modeling of photometric light curves provides a way to generate a large amount of data under controlled conditions for working the inverse problem and is an effective way to test Non-Resolved Space Object Identification (NRSOI) techniques. Currently there are two ways of generating this data. One is to use ray-tracing on a complex model of the satellite, a task which requires enormous computing power and time. The second way, which we are using here is to create simpler models of satellite bodies and use albedo-area calculations with the Cook-Torrance BRDF model. This is a much faster, albeit less accurate method.

		Form Approved OMB No. 0704-0188

Report Documentation Page

1. REPORT DATE **SEP 2009**	2. REPORT TYPE	3. DATES COVERED **00-00-2009 to 00-00-2009**

4. TITLE AND SUBTITLE **Simulating Complex Satellites and a Space-Based Surveillance Sensor Simulation**	5a. CONTRACT NUMBER
	5b. GRANT NUMBER
	5c. PROGRAM ELEMENT NUMBER
6. AUTHOR(S)	5d. PROJECT NUMBER
	5e. TASK NUMBER
	5f. WORK UNIT NUMBER

7. PERFORMING ORGANIZATION NAME(S) AND ADDRESS(ES) **U.S. Air Force Academy,Department of Physics,USAF Academy,CO,80840**	8. PERFORMING ORGANIZATION REPORT NUMBER

9. SPONSORING/MONITORING AGENCY NAME(S) AND ADDRESS(ES)	10. SPONSOR/MONITOR'S ACRONYM(S)
	11. SPONSOR/MONITOR'S REPORT NUMBER(S)

12. DISTRIBUTION/AVAILABILITY STATEMENT
Approved for public release; distribution unlimited

13. SUPPLEMENTARY NOTES
2009 Advanced Maui Optical and Space Surveillance Technologies Conference, 1-4 Sep, Maui, HI.

14. ABSTRACT
Maintaining space situational awareness requires the ability to track earth-bound satellites in order to know and predict their position, movement, size, and physical features. However, there are many satellites in orbit that are simply too small or too far away to resolve by conventional optical imaging. We can use photometric techniques to gather information about the body in question, but the problem comes in how we interpret the light curve data. Light curves are created by measuring the intensity of reflected sunlight off of the object as it passes overhead. The intensity is dependent on a variety of factors to include the size, shape, orientation, and material composition of the satellite. When we attempt to solve the inverse problem for light curves, we are attempting to extract information about these different factors. Forward modeling of photometric light curves provides a way to generate a large amount of data under controlled conditions for working the inverse problem and is an effective way to test Non- Resolved Space Object Identification (NRSOI) techniques. Currently, there are few implementations of such modeling programs, one of which only allows simple geometric shapes with the option of antennas. We present our modification to that existing code to create complex models plus our new code to calculate shadowing on the complex object. Then we show the results from the new model and a comparison to the original tool. The next generation of space surveillance sensors will be on satellites. Space based sensors avoid many of the problems of ground based sensors, such as, waiting for lighting conditions to match satellite passes and a night sky. These sensors are restricted only by sun exclusion angle and line of sight around the Earth. This allows for more effective techniques and a much longer time on target. We present an addition to the existing code to consider a sensor in orbit. The code is generalized to provide flexibility in testing different orbital parameters and provides pass prediction with predictive forward modeling for any orbit.

15. SUBJECT TERMS

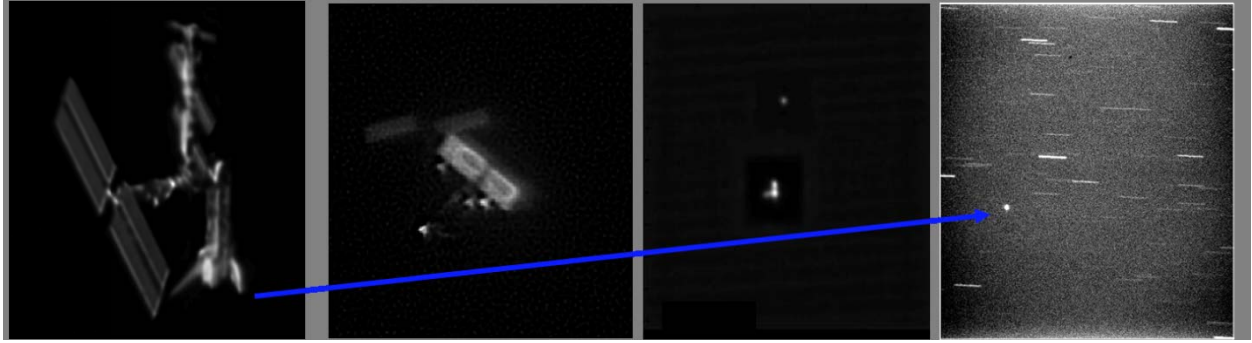| 16. SECURITY CLASSIFICATION OF:			17. LIMITATION OF ABSTRACT	18. NUMBER OF PAGES	19a. NAME OF RESPONSIBLE PERSON
a. REPORT **unclassified**	b. ABSTRACT **unclassified**	c. THIS PAGE **unclassified**	**Same as Report (SAR)**	**10**	

Fig. 1. Degradation of high-resolution images with increasing distance and/or decreasing satellite size.

The initial photometric modeling tool we started with was developed in MATLAB® by the Directed Energy Directorate of the Air Force Research Laboratory (AFRL). The simulation uses two line elements (TLEs) to determine satellite pass geometry and allows a user to define satellite size, shape, material, and attitude as well as observation location. This tool has been used in the past by AFRL to investigate various non-resolvable space object identification problems such as analyzing when single facets become visible or illuminated by the sun as viewed from closely spaced observers [1]. A version of this tool has also been used to investigate glints from cubesats [2]. The initial tool included very simple convex shapes such as cubes, rectangular parallelepipeds, N-sided cylinders, and other regular geometric shapes. We ask, can we learn more with complex bodies, or is it too difficult to extract information? In answering this question, we had to modify the software.

Our first task was to create a technique to combine the simple shapes (e.g. rectangular parallelepiped with rectangular solar panels) and make more complex structures. Once we had these complex bodies, we had to adapt the code for shadowing effects. Once this was done, we compared the new results to the old and to see if this is a viable model, and determine whether we can extract more information. We discuss this work in Section 2.

In addition to the complex body modeling, we felt it would be necessary to have a tool with which we can test different aspects of observing with a space-based sensor, which is especially poignant considering the potential space-based sensors planned for the future. We again modified the original photometric modeling tool to generate data for a space based sensor as it observed other satellites. This work is discussed in Section 3.

2. MODELING OF COMPLEX SHAPES

2.1. Computational Algorithm

To model the intensity of a satellite's photometric light curve, the current tool sums up the reflected light from individual facets of the simulated object for each time step in the run. The reflected light of course depends on the distance from the satellite to the sensor, the solar phase angle, the reflective properties of the facet, and the orientation of the facet with respect to the sun and the observer. Combining simple shapes into a more complex shape requires accounting for the shadowing from one part of the satellite onto another part. We attempt to reduce the overall facet intensity by subtracting out the shadowing area from the facet's albedo-area product.

When we began adapting the code for complex shapes, we found there were a few specific, major portions needed for the algorithm. We must find the facets which cause shadowing, calculate the area of the shadow, and subtract it from the reflectance area on the shadowed facet. Our algorithm begins by finding whether any facets which can cause shadowing are lit. These facets are previously specified by the user for the time being. The sun unit vector is used in body centered coordinates to project the lit "shadowing facets" into the planes of the facet for which we are currently calculating the intensity.

The vertices of the shadowing facet are now in the plane of the facet for which we're calculating the intensity. These vertices define the perimeter of the shadow, but are typically unordered. The Qhull algorithm is then applied to arrange the vertices in order that they appear on the perimeter. The shadowed facet is split into a grid of many

small squares and we find the intersection of the shadow polygon with the grid of the facet. Finally, the number of intersections is summed and multiplied by the area of each square in the grid, giving us the shadowed area.
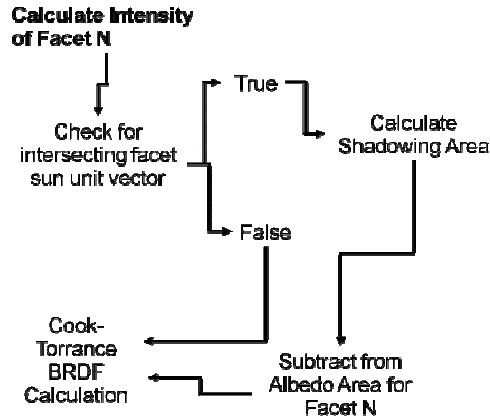

Fig. 2. Schematic flow for calculating the intensity for a given facet.

Out calculations were completed with two models, a control model that was a parallelepiped with 1m×1m×3m dimensions, a diffuse albedo of 0.3, and no specular reflection. The second model was an experimental, complex body model which had the control model dimensions as a main body with the addition of two face-perpendicular panels of 1m×3m×0.05m dimensions and with the same albedo. The experimental, complex body model can be seen in Figs. 3-5 at different orientations.

2.2. Analysis and Results

We present three different passes of our complex body which are just a sample of the total number of passes we simulated. These passes were simulated using parameters for the AEOS telescope on Mt. Haleakala with passes occurring at orientations of 9°, 45°, and 90° to the terminator. For the satellite attitude, we ran cases for both an axial spinner and a nadir-ram pointing stabilized body. We simulated a pass without the shadowing code implemented, followed by a pass with the shadowing code implemented, then compared the magnitudes reported for each time step to determine magnitude residuals. The residuals would show if our code is producing different results for the shadowing version compared to the non-shadowing version.

In all our passes aside from one (not shown here), the shadowing, or complex-body code does show a slightly different light curve from that of the non-shadowing code. While we believe not quantitatively correct, shows the correct behavior qualitatively. These residuals reach a maximum of 0.12 stellar magnitudes of difference from the non-shadowing lightcurves. We have not yet determined where the supposed error occurs, but can attribute it to a few possible sources. These will be discussed later.

The first pass (Fig. 3, Engagement #1) we present is for the complex body in an orbit associated with SSN Object 27842 (841 km altitude, 90.2° inclination, RAAN of 84.54°, and eccentricity of 0.0010). On March 28, 2009, there is a dawn pass observed from AEOS between 1537-1553 UT which crosses the terminator at a 9° angle. The satellite was given a spinning attitude along the axial direction. As seen in Fig. 3, the satellite begins with an orientation with its spin axis toward the observer. As the satellite moves through its orbit, it passes nearly overhead of AEOS and the observer begins to see the lit and shadowed side of the satellite, accounting for the seemingly late rise in periodic shadowing. Interestingly however, for most of the pass, the light curves of the controlled satellite and the experimental satellite are identical with zero residual. Only during the last third of the pass does one see non-zero residuals thus indicating a difference between the light curves.
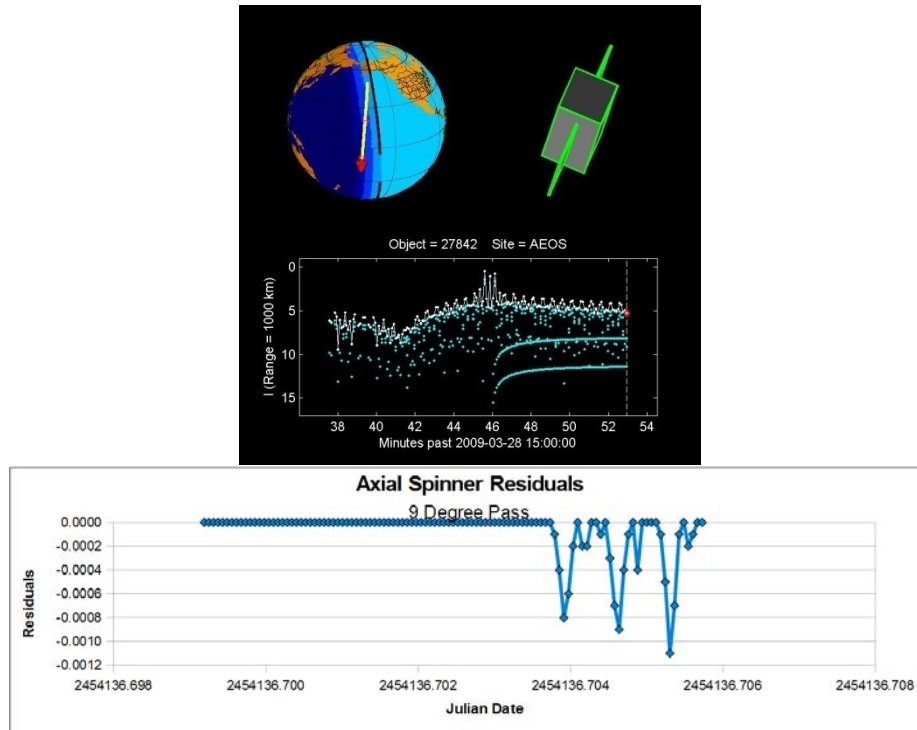
Fig. 3. Engagement #1. The top panel shows the simulated results of the photometric tool. The image of the globe includes the terminator, a sensor site indicated by the red plus sign, and the satellite pass in yellow moving from north to south. The complex body image is the orientation of the satellite as seen from the sensor site. The plot of intensity (I) versus time shows the overall intensity in white and individual facet intensities in blue. Finally, the bottom panel is a plot of residuals or difference between the complex body with shadowing and the complex body without shadowing.

The second pass (Fig. 4, Engagement #2) we present is for the complex body in an orbit associated with SSN Object 28773 (560 km altitude, 31.41° inclination, RAAN of 335.71°, and eccentricity of 0.0007). On February 5, 2007, there is a dusk pass observed from AEOS between 0430-0500 UT which crosses the terminator at a 90° angle. This satellite was also given an axial spinner attitude. Initially, the satellite begins the pass oriented with its spin axis toward the observer. The residuals in the first third of the light curve have a higher frequency than the actual rotation rate of the satellite, however the last two-thirds of the residual plot shows shadowing occurring at the rotation frequency of the satellite. Further analysis is required to understand the difference in the shadowing frequency.
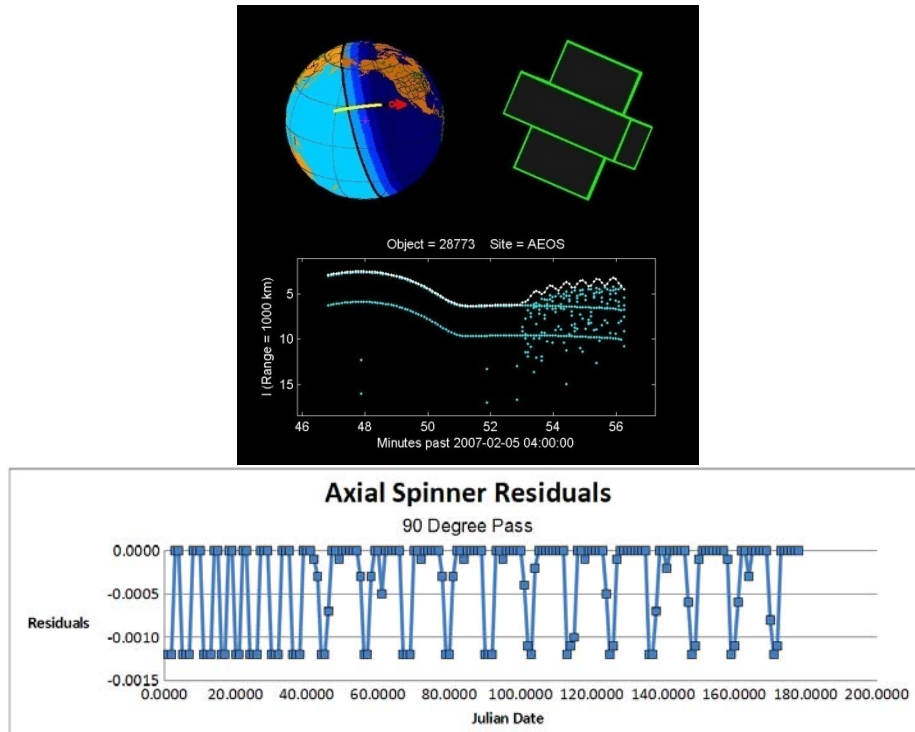
Fig. 4. Engagement #2. Same format as Fig. 3.

The final pass (Fig. 5, Engagement #3) we present is for the complex body in an orbit associated with SSN Object 27844 (1171 km altitude, 42.2° inclination, RAAN of 83.55°, and eccentricity of 0.0011). On March 13, 2009, there was a dawn pass observed at AEOS between 1545-1558 UT which crosses the terminator at a 45° angle. Contrary to the previous cases, this satellite was in a nadir-ram stabilized attitude with its body *x*-axis pointing to the ram and its body *z*-axis pointing to nadir. For this engagement, the satellite begins the pass oriented with its ram axis nearly toward the observer. As the satellite moves through its orbit, the observer begins to see an increasing and systematic shadowing effect as indicated in the residual plot. One does not see any periodic shadowing due to satellite spin since the satellite is not spinning. Additionally, as the satellite passes the observer and across the terminator, the "solar panel" appendages appear to reduce the overall intensity from the side facets of the main body as one would expect.
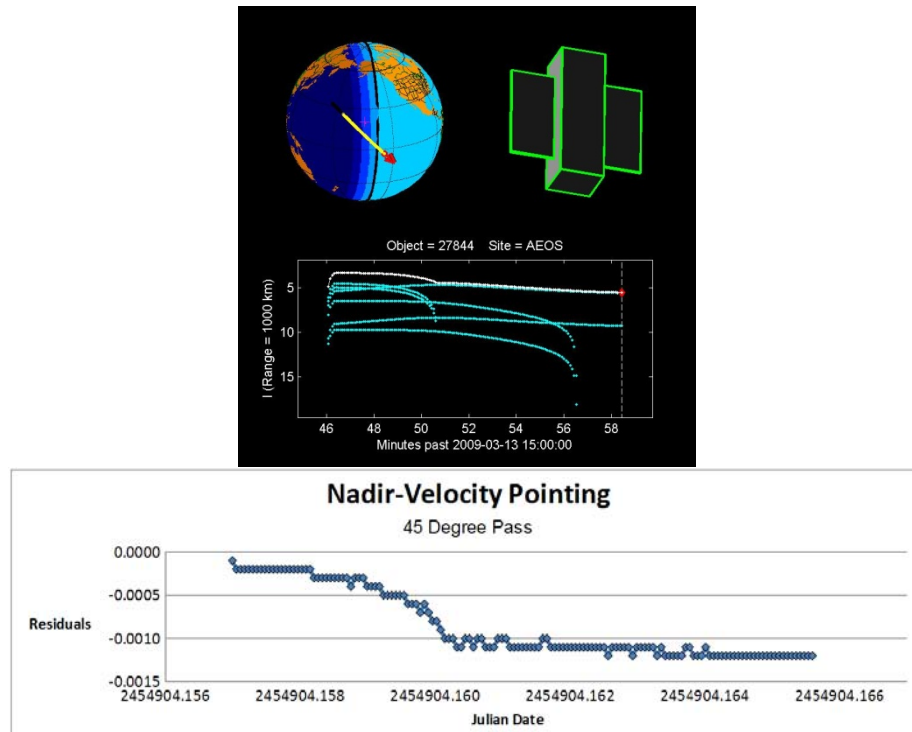
Fig. 5. Engagement #3. Same format as Fig. 3.

We may draw three basic conclusions from this data shown above. First, the shadowing code appears to account for one facet shadowing another facet. Second, the shadowing effect appears consistent with the satellite attitude as seen by the marked differences in the residuals between the axial-spinner and nadir-ram pointing attitudes. Finally, we were able to "measure" the shadowing effect by comparing a complex body with shadowing to one without shadowing. However, when observing an actual satellite in orbit and measuring its time-varying photometric light curve, one must devise a way to determine whether the object is indeed a complex shape exhibiting shadowing, or a simple object with no shadowing.

3. SPACE-BASED SENSOR MODELING

3.1 Pass Prediction and Visualization

The photometric tool created by AFRL and modified as described above to accommodate complex shapes has one limitation. Currently, it can only model satellites as observed from fixed ground sites. Theoretically, this tool can model a sensor site at a fixed longitude and latitude, but at an altitude representative of a satellite orbit. Of course, in doing so, one does not even come close to modeling the effects of the sensor movement on the target's photometric light curve. With future space-based sensors planned, we decided to modify the AFRL tool to model a satellite's photometric light curve as measured by another orbiting satellite. Most of the tool's functions and routines were still applicable, except that now we had to modify the code to accept orbit parameters for the sensor satellite and predict when the sensor satellite will be able to observe the target satellite under various constraints such as a sun-exclusion angle and no measurements against the hard earth background.

The first step in the modification was to rewrite the pass prediction code. The current pass prediction algorithm takes two-line elements (TLEs) of the observing satellite and propagates them using SGP4. It then finds the TLEs of the target satellite and propagates it using the observing satellite's coordinates as the "ground observer" coordinates. Once both orbits were propagated, we had to calculate all ephemeris points where the Earth and the sun

excluded the view of the target. The ephemeris where the target was actually lit was previously calculated by the original code, so no modification of this aspect was necessary.

Once the accepted passes were computed, we needed a way to visualize them. There are two basic methods for visualization of the geometry. The first is a three-dimensional view from far away, the "globe" visualization shown in Fig. 6. It is interactive with the user able to rotate the view to any angle and the celestial sphere projected to the Earth's surface for sky location reference. As seen in Fig. 6, the satellite sensor's orbit is indicated by the blue trace while the target satellite orbit is the red-yellow trace. For this case, the satellite sensor was in a higher altitude orbit than the target satellite. That portion of the target satellite orbit that cannot be viewed by the satellite sensor is in red while the portion that is viewable is in yellow. The sun unit vector is indicated by the orange arrows from the target satellite orbit. The globe visualization also shows a green line from the satellite sensor to the target satellite for reference. One can see that for most of the target satellite orbit, the satellite sensor can observe the target satellite. It isn't until the end of the orbit does the hard-earth background exclusion restrict the viewing.
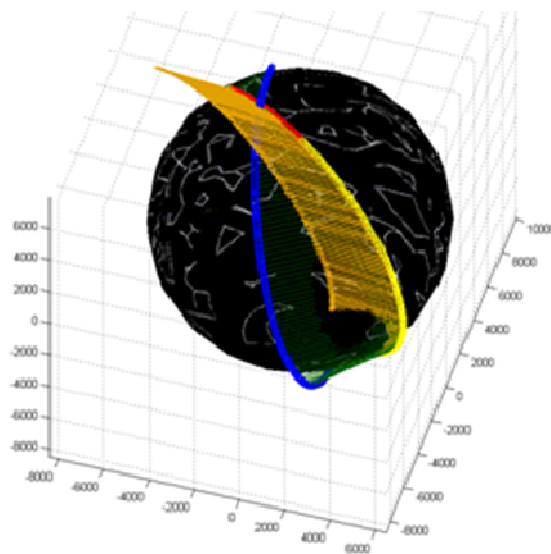

Fig. 6. Globe visualization of the viewing possibility (in RA-Dec projection) for a satellite sensor looking at a lower altitude target satellite. The orbital path of the satellite sensor is dark blue. The orbital path of the satellite target is yellow when viewing is possible and red when it is not possible. The sensor-to-target vector is green and the Sun unit vectors are orange arrows.

The second visualization method plots the orbital paths on a right ascension, declination (RA-Dec) Mollweide projection along with the vector pointing from the sensor to target and the location of sun exclusion. Fig. 7 shows the same orbital data as in Fig. 6 with the Earth located in the center. The orbital path of the satellite sensor is light blue when viewing is not possible and dark blue when possible, while the orbital path of the target satellite is black when viewing is not possible and red when possible. The beginning the orbits are indicated by the green squares. The sensor-to-target vector is green and the Sun's location and exclusion area is yellow. One can see that at the beginning of the orbits, the satellite sensor cannot view the target satellite due to the restriction of viewing against the hard earth background.
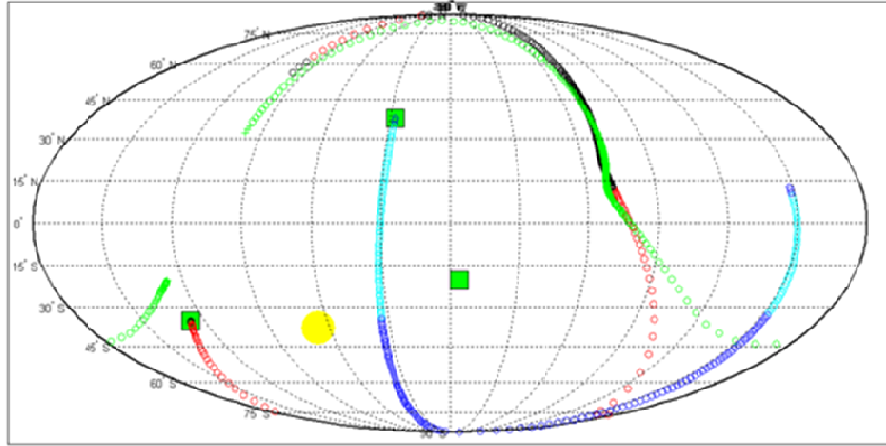
Fig. 7. Visualization of the viewing possibility in RA-Dec Mollweide projection with the Earth in the center. The orbital path of the satellite sensor is light blue when viewing is not possible and dark blue when possible, while the orbital path of the target satellite is black when viewing is not possible and red when possible. The green squares indicate the beginning of the orbits. The sensor-to-target vector is green and the Sun's location and exclusion area is yellow.

We found the pass prediction to be the most computationally intensive part of the code, typically taking 90-95 percent of runtime depending on other selected options. For example, a pass prediction for six months took approximately six hours. We added a feature to save the pass information to a file so that one can then load it if one wanted to simulate different satellite shapes for the same passes, thus saving time and obtaining results faster.

Once the basic pass prediction functionality was completed, we moved on to modification of the photometric modeling. All that was required was to calculate the vector from the sensor to the target and pass that into the bidirectional reflectance distribution function (BRDF) calculation as the observation vector. Doing so would require minimal change to the BRDF calculation code. However to do so, we had to first propagate the satellite sensor's orbit, followed by the target satellite's orbit, using the ECI coordinates of the satellite sensor as the observer coordinates.

3.2 Photometric Data from a Space-Based Sensor

Once the modifications to the original software was complete, we ran test cases to verify that the modifications were producing correct results. Earlier research has shown that the phase angle-magnitude distribution for various shapes have a characteristic differences [1]. Specifically, it appears that every object has a distinct lower bound brightness curves that depend only on the shape of the object and not on its size or material properties. For instance, cubes show a distinct diffusive cutoff angle at 90° solar phase angle corresponding to the face of the cube visible to an observer being 90° to the sun. For a tetrahedron, the cutoff solar phase angle is 54.7° (or $\overline{}$) corresponding to the angle between a face and an edge [3]. Cylinders have two lower bound or minimum intensity curves with asymptotes of 90° and 180° corresponding to the end caps and cylindrical sides, respectively. We ran six months of passes for each of three shapes: cube, tetrahedron, and cylinder. Each of these were also run as a purely diffuse object with albedo of 0.3, and separately with an analytical BRDF with diffuse albedo of 0.3 and specular albedo of 0.15, for a total of 6 cases.

All runs of the six cases appeared to produce phase angle-magnitude distributions as expected. We plotted approximately 300 different passes for each case, which gave a very wide distribution of phase angles. Two of these plots, one of a cube with specular component and the other a purely diffuse cylinder are shown in Fig. 8. All showed the defined lower bound curves which appear to asymptote to dimmer magnitude at the correct phase angles. This feature is more evident in the cube than the cylinder data. The cube which had a specular component also showed intensities brighter than the lower bound curve as expected. There are however some unexpected data points below the lower bound curve which we are currently investigating.
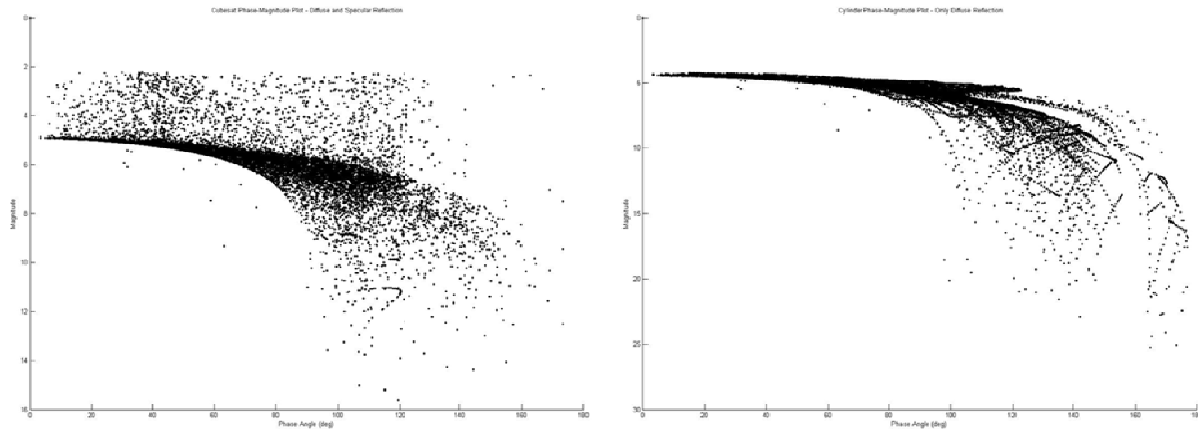
Fig. 8. Phase angle-magnitude distributions for a cube (left plot) and cylinder (right plot) from 300 passes. The phase angle is the *x* axis while the magnitude is the *y* axis. Notice the structure from the specular component on the cube compared to the purely diffuse cylinder.

In our testing, we noticed the orbital sensor has the inherent property of a wider coverage of phase angles for every observation pass. This is due to the satellite sensor moving much faster and farther during a pass than a ground-based sensor would. Additionally, because of the wide geometry changes inherent in the orbits passing each other, an orbiting sensor sees many more target satellite attitudes than a ground-based sensor, especially when the target is in a stabilized nadir-ram pointing attitude. Since it appears that phase angle-magnitude distributions can be used to determine satellite shapes, the more phase angle coverage one can obtain to discern the lower bound curve, the higher confidence one can have in the identification. Additionally, because of the wider coverage of phase angles and attitudes on each pass, an orbiting sensor could potentially allow for quicker identification of shape for unknown satellites than a ground based sensor.

4. CONCLUSIONS

Modifications to an existing photometric tool to allow for complex satellite shapes and a space-based sensor appear to be working properly. There is still however some analysis required to fully understand the simulated photometric light curves. For the shadowing model, future work would include creating more and different types of composite bodies, finding a method to generally call the shadowing function, and creating a generalized composite body GUI. For the space-based sensor model, future work includes combining it with the shadowing version, researching time-on-target for different classes of orbits, classifying available coverage for different classes of orbits, and developing metrics to define these aspects.

5. ACKNOWLEDGEMENTS

6. REFERENCES

1. Hall D. et. al., "Separating Attitude and Shape Effects for Non-resolved Objects," *The 2007 AMOS Technical*

Conference Proceedings, Kihei, HI, 2007.

2. Hall D., "Optical CubeSat Discrimination," *The 2008 AMOS Technical Conference Proceedings*, Kihei, HI, 2008.

3. "Tetrahedron." *Wikipedia, The Free Encyclopedia*. 26 Aug 2009, 21:44 UTC. 26 Aug 2009 <http://en.wikipedia.org/w/index.php?title=Tetrahedron&oldid=310245038>.